

Field measurements of cable self-burial in a sandy marine environment

Unsworth, Christopher; Austin, Martin; Van Landeghem, Katrien; Couldrey, Amelia; Whitehouse, Richard; Lincoln, Ben; Doole, Siobhan; Worrall, Peter

Coastal Engineering

DOI:

[10.1016/j.coastaleng.2023.104309](https://doi.org/10.1016/j.coastaleng.2023.104309)

E-pub ahead of print: 01/09/2023

Publisher's PDF, also known as Version of record

[Cyswllt i'r cyhoeddiad / Link to publication](#)

Dyfyniad o'r fersiwn a gyhoeddwyd / Citation for published version (APA):

Unsworth, C., Austin, M., Van Landeghem, K., Couldrey, A., Whitehouse, R., Lincoln, B., Doole, S., & Worrall, P. (2023). Field measurements of cable self-burial in a sandy marine environment. *Coastal Engineering*, 184, [104309]. <https://doi.org/10.1016/j.coastaleng.2023.104309>

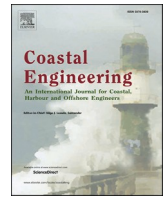
Hawliau Cyffredinol / General rights

Copyright and moral rights for the publications made accessible in the public portal are retained by the authors and/or other copyright owners and it is a condition of accessing publications that users recognise and abide by the legal requirements associated with these rights.

- Users may download and print one copy of any publication from the public portal for the purpose of private study or research.
- You may not further distribute the material or use it for any profit-making activity or commercial gain
- You may freely distribute the URL identifying the publication in the public portal ?

Take down policy

If you believe that this document breaches copyright please contact us providing details, and we will remove access to the work immediately and investigate your claim.



Field measurements of cable self-burial in a sandy marine environment

Christopher A. Unsworth^{a,*}, Martin J. Austin^a, Katrien J.J. Van Landeghem^a,
Amelia J. Couldrey^b, Richard J.S. Whitehouse^b, Ben Lincoln^a, Siobhan Doole^c, Peter Worrall^c

^a School of Ocean Sciences, Bangor University, Menai Bridge, Isle of Anglesey, LL59 5AB, United Kingdom

^b Coasts and Oceans, HR Wallingford, Kestrel House, Howbery Park, Wallingford, OX10 8BA, United Kingdom

^c JDR Cables Victoria Dock, Greenland Rd, Hartlepool, TS24 0RQ, United Kingdom

A B S T R A C T

The world's shallow continental shelves are currently experiencing a rapid pace of development from the growth of offshore renewable energy. The emplacement of infrastructure on the seabed can change the morphology of the bed, the nature of the flow above it the transport of sediment, and so complicate the assessment of seabed stability for planning and designing offshore renewable infrastructure. To ascertain how much of an impact these natural processes have on the stability of cables, we present the first field observations made directly over a section of subsea cable, from two deployments in the Eastern Irish Sea at a location of current and planned offshore windfarms. Profiles of flow, turbulence and suspended sediment concentration were measured over a section of typical high voltage electricity cable. Upon deployment our observations showed that sediment was deposited around the cable and self-burial occurred. The rate of deposition varied between surveys dependent on forcing and local bed conditions. Turbulence generated from the cable itself reduced as the embedment depth increased, but the relationship between bed shear stress and suspended sediment concentration was not consistent between surveys. We discuss several processes potentially responsible for the prevalence of deposition around the cable, and the difference in seabed mobility between the surveys.

1. Introduction

The cables that underpin the transfer of energy and data across the sea floors are vulnerable to the impacts exerted by a mobile and dynamic seabed. The exposure and subsequent damage from fishing, anchors, or abrasion during sediment transport can disrupt communication and critical infrastructure (Ardelean & Minnebo, 2023; Clare et al., 2023). There are a number of risks to infrastructure stability in the marine environment, from excess burial of high voltage cables causing overheating and reduction in transmission capacity to sea floor scour and bedform migration leading to cable exposures. For offshore windfarms crucial to the green energy transition, power cable repair in the United Kingdom (UK) alone costs between £1.3M (per inter-array cable) and £27M (per export cable) and takes 40–60 days to complete. Subsequent loss claims are estimated to account for >40% of UK Offshore Renewable Energy (ORE) insurance claims. Cable claims make up 83% of all claim's costs, with vessel costs a major factor. Between 2014 and 17 in the UK, cable failure led to a cumulative loss of power generation of ~2.45 TWh, equating to ~£250M (El Mountassir and Strang-Moran, 2018). Based on recent analysis 57 of the last 60 construction projects in the UK experienced cable failure, suggesting that occurrences and associated disruption and costs will increase as the number of windfarms and wind turbines increases over the next decade.

Cables can become exposed and suffer fatigue loading due to self-induced scour of the seabed, causing the cable to sag and vibrate when unsupported (Mayall et al., 2020; Sumer et al., 2001a, 2001b; Zhang et al., 2021); a similar affect can happen due to the passing of bedforms, leading to local scour around a section of a cable (Couldrey et al., 2020; Damgaard et al., 2015). The onset of cable scour caused by uni-directional currents can be predicted using the cable's Shields type parameter (Sumer and Fredsøe, 2001, 2002);

$$\frac{U_{cr}^2}{gD_c(1-n)(s-1)} = 0.025 \exp \left[9 \left(\frac{e_c}{D_c} \right)^{0.5} \right] \quad \text{Eq. 1}$$

where U_{cr} is the mean current required for the onset of scour under the cable, defined at the top of the cable and n is porosity of the seabed (= 0.4), g is acceleration due to gravity (assumed 9.81 m s^{-2}), s is the relative density of sediment in water ($s = \rho_s/\rho_w$), D_c is the diameter of the cable and e_c is the embedment depth. Flows in mobile sedimentary environments less than the critical velocity for onset of scour should lead to deposition, with scour occurring once flows exceed the threshold (Fig. 1).

Whilst seabed mobility is often included in the design and placement of seafloor cables around offshore windfarms, it is often unclear why cables will either scour or self-bury through natural marine processes

* Corresponding author.

E-mail address: christopher.unsworth@bangor.ac.uk (C.A. Unsworth).

(Whitehouse and Draper, 2020). One possible cause could be the turbulence generated by the cables themselves - which depending on the environmental conditions will either induce erosion or deposition of sediment around the cable. Such morphological alternation of the local environment by the cable itself is often not included in an assessment of cable stability at the site as cable design is often concerned with cable scour through piping, tunnel scour and liquefaction (Sumer and Fredsøe, 2001; Sumer and Kirca, 2022). Recent field surveys have revealed that cables and pipelines can self-bury due to the drag on the flow acting as a sediment attractor (Leckie et al., 2016), and not just as a cause of scour (cf. Sumer et al., 2001a). There are examples where high levels of suspended sediment will result in deposition, rather than erosion and scour, even when the hydraulic conditions would otherwise indicate scour formation (Leckie et al., 2018; Zhao et al., 2015), suggesting that additional processes need to be accounted for when estimating the onset of scour.

In a highly mobile environment, it is difficult to define the range of conditions a cable may experience due to the varying scales of induced turbulence from the infrastructure itself and from the passage of migrating bedforms; both can affect the reference velocity used to estimate the potential for scour (Couldrey et al., 2020). Turbulence and mean velocity can change dramatically over a single bedform - greatly affecting shear and bed shear stress at a local (metre) scale (Bennett and Best, 1995; Dey et al., 2020; Unsworth et al., 2018). The overall bed mobility can also change spatially over sub-tidal bedforms due to biological modification of the seabed (Damveld et al., 2018) or via the reversing tidal flow mobilising sediment just at bedform crests (Lefebvre et al., 2022), which further complicates prediction of seabed mobility and sediments response to the induced turbulence from offshore infrastructure. Waves also have a moderating effect on scour, but also on near bed suspended sediment concentration and seabed cohesion, adding a temporal (through storms) and spatial (location of the wave base) variability to their effects on the seabed. Much of the laboratory work which underpins cable-seabed interaction has focused on identifying the onset of scour (e.g. Sumer et al., 2001a; Sumer and Fredsøe, 2001, 2002) rather than the morphodynamics induced by periodic tidal conditions (e.g. Leckie et al., 2016). Yet, dynamic feedbacks between flow, the suspension of sediment, and deposition around the cable do exist (Leckie et al., 2015, 2016, 2018). For example, deposition around the cable and increasing embedment depth (e_c) creates positive feedback which reduces the amount of induced turbulence shed from the cable - and subsequently decreases the likelihood of scour. Clearly, field surveys are needed to see how the natural complexity of these environments can affect our present understanding of cable scour processes, particularly the time-dependent nature of these processes.

The aim of this paper is to quantify what role seabed mobility, suspended sediment concentration and locally produced turbulence have

on modifying the existing relationships for the prediction of cable scour. We hypothesise: (1) that the turbulence and sediment suspension induced from offshore renewable infrastructure can alter these relationships; and (2) that high levels of suspended sediments found in tidally energetic environments promote deposition, rather than erosion, around cables (Fig. 1). We use field observations made in a shallow tidally energetic environment to quantify both the flow and sediment dynamics over a section of subsea cable using multiple acoustic profiling instruments. We take advantage of different flood and ebb flow regimes caused by the careful design and deployment of our instrument lander to quantify the impact of the self-generated lee wake on the mean and turbulent flows across the cable and their subsequent control on cable burial.

The paper is organised as follows. After brief reviews of the field site and methods (Section 2), we present the results (Section 3). This is followed by sections based on more detailed analysis of the data (Section 4), which focuses on the effect of varying embedment depth on: (1) exploration of the timing of bed level changes around the cable, (2) the hydraulic conditions the cable experienced in relation to Eqs. (1) and (3) the effects of drag and turbulence produced the cable. The paper concludes with a discussion and summary of the results.

2. Methods, field site, and deployment

2.1. The study site

The study site was on the *Constable Bank* in the Irish Sea 6 km off the coast of North Wales, UK (53° 22.5616' N, 3° 43.6308' W, Fig. 2). The site is close to existing and proposed offshore windfarms and their cables, so the surveys are highly representative of the active and future offshore renewable energy environment. The site has a semi-diurnal macro tidal regime, mean tidal ranges of 7.2 m at springs and 3.8 m at neaps (measured at *Llandudno*, <https://ntslf.org>). The tidal wave is standing, and dominant flood and ebb directions (from North) are 100° and 270–290°, respectively, with directions typically more consistent during floods than ebbs, as rotation of flow at slack tide lags due to the inertia of flow into Liverpool Bay. Median wave heights measured from the Rhyl Flats wave rider (coastalmonitoring.org) over the period 2007–2021 are 0.57 m, with 90th and 99th percentile significant wave heights of 1.39 m and 2.42 m, respectively. Significant wave periods are typically short, with a median of 4 s, and 6.7 s at the 99th percentile. Dominant wave directions are between 300° and 350°, with a maximum fetch of 160 km.

2.1.1. The data collected

The project saw two offshore surveys of the Constable Bank (Table 1), during which a seabed lander was deployed, and seabed

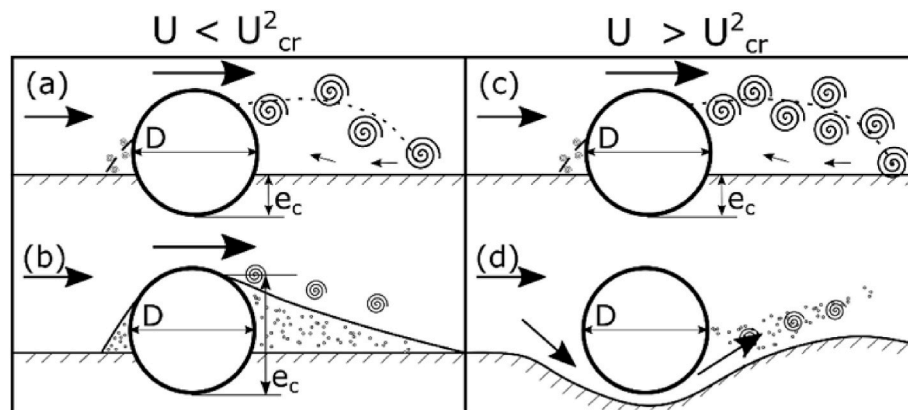


Fig. 1. Conceptual diagram of cable-seabed interactions under different hydraulic and sediment regimes. (a) and (b) represent before and after responses to flow separation over a cable when $U < U_{cr}^2$ the threshold outlined by Eq. (1). Whilst (c) and (d) represent what happens in the hydraulic regime.

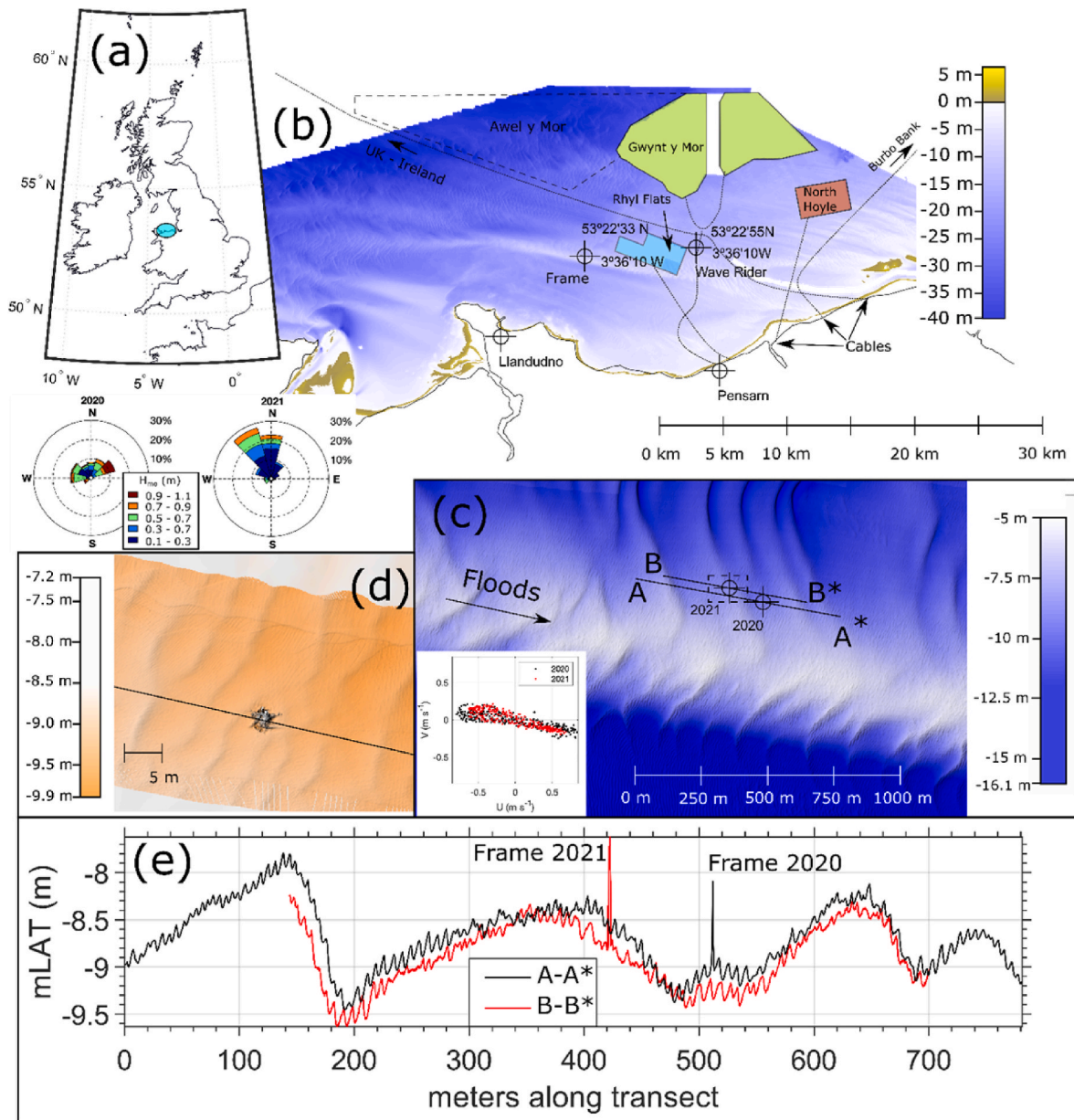


Fig. 2. (a) Geographic projection of the UK and Ireland, with the location of the site of interest in light blue, with an inset of the wave roses for each deployment. (b) North Wales coastline and 2 m resolution bathymetry with existing wind farms in coloured polygons and proposed wind farms in dashed. Electric cables are indicated with dotted lines. (c) Close up of Constable bank, with the transects A and B shown – these lines are also parallel to the mean flood tide direction at the site (inset shows measured tide directions), lander deployment locations and the outline of (d) shown with dashes. (d) Close up of the deployment lander in 2021 with a 0.1 m resolution MBES line (orange to white) measured during the deployment. (e) Transects showing multiple bedform scales and the lander locations. 2020 MBES data, collected on September 23, 2020, 2021 MBES data collected on July 15, 2021.

Table 1

Dates of surveys.

Dates	Location of the lander
18/9 -> September 19, 2020	Lat: 53° 22' 32.3295 Lon: -3° 43' 36.0741
20/9 -> 23/9/2020	Lat: 53° 22' 32.7459 Lon: -3° 72' 34.8921
14/7 -> 18/7/2021	Lat: 53° 22' 33.9122 Lon: -3° 43' 39.9091

bathymetry data was continuously collected using a vessel mounted Multibeam Echosounder (MBES) over the lander site. In the 2020 deployment the lander was positioned twice to try and gain repeated

measurements of the initial flow and sediment transport response to the lander being positioned on the seabed. The 2021 survey was only one deployment, for a longer time period.

Fig. 2d–e provides a close-up of the seabed morphology as measured during the lander deployments and inset of the outline of the lander as seen by the MBES. The seabed lander, fitted with instrumentation as well as a section of seabed electricity cable (diameter $D_c = 200$ mm), was deployed from the RV Prince Madog at the end of an ebb tide. The front end of the lander supporting the cable faced into the dominant flood direction so that data collected during flood tide measured the natural flow (unaffected by the presence of the cable or lander), whilst data collected during ebb tides would be measuring the self-generated turbulent wake from the lander and cable (Fig. 3). Instrumentation setup details relevant to the current study are given in Table 2. Seabed

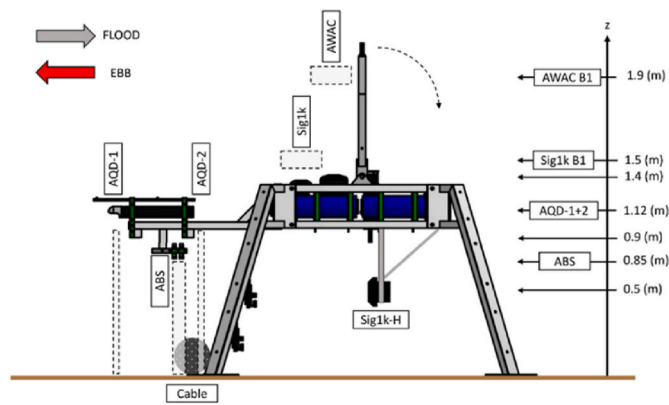


Fig. 3. Schematic of the instrument lander and the location of instrumentation fixed to the lander. Dashed outlines indicate location of measurements used in the survey, “B1” indicates the location of the first bin of data. The section of cable is fixed to the base of the left side of the lander. Upon deployment, the arm at top of the lander swings down to the right upon release of the crane hook and the Sig1k and AWAC results are not affected by this arm. The Sig1k-H results are not used in the current paper.

sediment grain size distribution was measured from analysing Shipek grab samples collected immediately prior to deployment of the lander in 2021. Samples were washed and dried overnight at 80 °C and dry sieved and weighed following the British Standard protocol (BS1377), with fines (<63 μm) collected onto pre-weighed filter paper, dried and weighed. Summary data are given in Table 3, with full details in appendix Table S1. Grain sizes are very consistent between surveys, with a 2 μm difference in median grain size. The ends of the distribution (D₁₀ and D₉₀) are slightly boarder in 2020 than 2021, but well within the same fine to median sand size range. The percentage of fines (<63 μm) is higher in the 2021 survey, but still less than 1% of the sample mass, indicating that there was little to no effect on sediment threshold of motion due to fines (Mohr et al., 2016) in either survey.

2.2. Data processing

The 600 kHz Nortek AWAC was deployed to quantify mean wave and current conditions during the surveys (Table 1, Fig. 3). The data were processed by the onboard Prolog unit to derive the integrated directional spectral wave characteristics via the acoustic surface tracking method. This method also provides the near-surface current speeds. A small compass heading offset adjustment was performed in post-processing using information from the more accurate motion reference unit in the Signature1000.

The lander mounted an array of acoustic devices for measuring currents and suspended sediment concentrations, diagrammed in Fig. 3. The Nortek Signature and Aquadopps were set to record in beam coordinates so that beam-based methods of estimating Turbulent Kinetic Energy (TKE) and Reynolds stresses could be used to then estimate turbulence production and dissipation (Guerra and Thomson, 2017; Rippeth et al., 2002). The combination of upward and downward facing

Table 2
Instruments deployed and setup information.

Instrument	Orientation	Mounting elevation	Vertical bin height	Measurement frequency	Burst length (Rest interval)
Nortek AWAC (600 kHz)	Upward facing	1.5 m	1 m	1 Hz (currents and waves)	Currents: 1 min (10 min) Waves: 8.5 min (20 min)
Nortek Signature ADCP (1 MHz)	Upward facing	1.4 m	0.5 m	8 Hz	10 min (30 min)
2x Nortek Aquadopp (1 MHz)	Downward Facing	1.13 m	0.05 m	2 Hz	10 min (30 min)
Aquatec Aquascat (ABS) 2020 : 1, 2, 4, 5, MHz 2021 : 1, 2, 2.25, 4, MHz	Downward Facing	0.85 m	2020: 0.01 m 2021: 0.005 m	64 Hz, internally averaged to 4 Hz	10 min (30 min)

ADCP’s allows for the mean and near bed flow structure to be measured, including any effects from the bedforms on the flow field as well as the effects of the cable and instrument lander on the ebb tide velocities, especially near the bed. Standard thresholds for correlation and amplitude were set for ADCP’s, which removed <5% of data, velocity spikes were filtered out using a gradient threshold of 0.14 m s⁻². Removed values were replaced with linearly interpolated values, if the gap between good values was smaller than 4 data points. Velocities were converted to XYZ (Cartesian coordinates) and ENU (East, North and Up coordinates) in post processing. Rotation to a local three-velocity component (UVW) coordinate system was performed using the median flood tide direction for each instrument, so that \bar{U} is maximised and \bar{V} over time is minimised, and underwent a Reynolds decomposition into burst-mean (with overbar) and turbulent components (with prime) commensurate to our tidally dominated site

$$U = (\bar{U} + u') [v; w] \tag{Eq. 3}$$

Bed shear stress τ_b was calculated from the turbulent velocity components following (Soulsby and Dyer, 1981):

$$TKE = 0.5\rho(\overline{u'^2} + \overline{v'^2} + \overline{w'^2}) \tag{Eq. 4}$$

$$\tau_b = 0.19TKE \tag{Eq. 5}$$

This has been shown to be the most accurate and reliable method of estimating bed shear stress in complex flows with localised point sources of shear and strong lateral gradients (Biron et al., 2004; Kim et al., 2000; Pope et al., 2006; Williams et al., 1999).

The Aquatec Aquascat Acoustic Backscatter System (ABS) was also deployed in downward facing orientation with 4 transducers to allow for the coincident measurement of flow and suspended sediment profiles. Scattering characteristic of the suspended sediments was estimated using the measured grain size distribution of the sediments with the method of Thorne and Meral (2008). Due to interference from the Aquadopp with the 1 and 2 MHz frequencies of the ABS, a multifrequency approach wasn’t possible – so the ensemble average method of inverting the ABS backscatter was employed (c.f. Thorne and Hanes, 2002) with good agreement (within 10% concentration) between the higher frequencies which are not affected from the noise from the Aquadopp instrument.

Seabed bathymetry data were collected using a hull mounted Reson SeaBat T50 echosounder, using the highest frequency in the available range (400 kHz). Tidal corrections and corrections for the pitch and roll movements of the vessel were applied while processing the datasets

Table 3
Summary data from bed sediment samples.

	2020	2021
% of samples <0.063 μm by dry weight	0.09%	0.22%
D ₁₀ (μm)	188	196
D ₁₆ (μm)	201	211
D ₅₀ (μm)	243	245
D ₈₄ (μm)	281	271
D ₉₀ (μm)	293	279

using the Teledyne PDS 2000 software. The processed gridded data have a grid cell size between 5 cm and 20 cm.

Bed sediments are a fine sand with a D_{50} of 243 μm in 2020 and 245 μm in 2021, with D_{90} 's of 293 μm and 279 μm for both years. Thresholds of motion (θ_{crit}^*) and suspension (θ_{sus}^*) were calculated via the modified Shields curve (Soulsby, 1997):

$$D^* = D_{50} \left(\frac{(S-1)g}{\nu^2} \right)^{1/3} \quad \text{Eq. 6}$$

$$\theta_{crit}^* = \frac{0.3}{1 + 1.2D^*} + 0.055 \{1 - \exp(0.02D^*)\} \quad \text{Eq. 7}$$

where g is the acceleration due to gravity, ν is the kinematic viscosity of the sea water (at 15 °C, $1.1384 \times 10^{-6} \text{ m}^2 \text{ s}^{-1}$ and $s = 2.58$ for quartz grains in seawater. The threshold for suspension is defined via (cf. van Rijn, 1993; Soulsby, 1997):

$$\theta_{sus}^* = \frac{0.3}{1 + D^*} + -0.1 \{1 - \exp(-0.05D^*)\} \quad \text{Eq. 8}$$

At winter temperatures of 5 °C, θ_{crit}^* for the sediments is 0.05 (0.2 N m^{-2}), and θ_{sus}^* 0.074 (0.29 N m^{-2}). At typical summer temperatures of 15 °C, θ_{crit}^* is 0.044 (0.18 N m^{-2}), and θ_{sus}^* 0.07 (0.27 N m^{-2}), indicating that seasonal variations in temperature account for a 12% difference in sediment mobility; the small difference in D_{50} between surveys produced a difference of <0.1%.

3. Results: Morphology of the seabed and water column during deployments

The seabed bathymetry data at Constable Bank consists of sedimentary bedforms of two main scales. The larger scale bedforms in and around the lander site have an average length of 194 m by 0.94 m high (range from 0.8 to 1.5 m high, 200–300 m long), and have an orientation of 150° (Fig. 3). Superimposed on these larger bedforms are smaller dunes of a scale 19 m long and 0.16 m high with a dominant angle of 100°, which is in line with the dominant flood tide direction. The location of the smaller bedform crests changed less than 0.1 m between the surveys in 2020 and 2021. Their shape changed during the tides in a similar way to estuarine bedforms (Lefebvre et al., 2022) where the location of the crest changed with tidal reversals, but the troughs did not. The size, shape and orientation of these smaller bedforms indicates there would be no/or little significant flow separation from the larger host bedforms (Herbert et al., 2015). The height of the larger bedforms is roughly equal to the height of the instrument frame (1.4 m) so near bed flows measured by the lander are within the turbulent boundary layer generated from the bedforms (Dyer, 1986; McLean et al., 1999; Nowell and Church, 1979).

The September 2020 deployment occurred during the autumnal equinox, producing some of the largest tides of that year. The deployment began during spring tides with water depths ranging between 9 and 17 m and associated high mean velocities of 0.75–1 m s^{-1} (Fig. 4a, c). Conditions transitioned to neap tides at the end of the survey with water depths of 10–16 m and velocities in the range 0.85–0.6 m s^{-1} . The 2021 survey was during a smaller spring neap cycle, 10–16 m water depth, with velocities peaking at 0.7 and reducing to about 0.5 m s^{-1} (Fig. 4b,d); the tidal ranges surveyed are typical of peak (2020) and average (2021) annual tidal forcing.

Wave activity peaked during the start of the 2020 survey with $H_{m0} = 1 \text{ m}$ and $T_{m02} = 3.5 \text{ s}$ (Fig. 4e, g), reducing to $H_{m0} < 0.5 \text{ m}$, before again peaking towards the end of the survey with $H_{m0} = 0.6\text{--}1 \text{ m}$. Long term (2007–2021) wave buoy data from the Rhyl Flats wave rider shows that 1 m high waves have an exceedance of 80%, indicating that these waves are relatively common in any given year. The 2021 surveys were mostly very calm with $H_{m0} < 0.4 \text{ m}$, except across the first two tidal cycles at the start of the survey where $H_{m0} = 0.7 \text{ m}$ and $T_{m02} = 3.5 \text{ s}$ (Fig. 4f, h). Flood

tide direction was a consistent 100° (Fig. 4i and j), whilst ebb tides show a rotation between 320° and 270°, typical of the flood dominant tidal conditions in the bay. Wave directions were rarely aligned with the tides during the surveys, with the main wave events arriving from a more northerly direction, suggesting the net bed shear stress direction under combined flows will be deflected southwards. The hydrodynamics during the surveys were therefore typical of average to peak tidal forcing conditions, with average to calm wave conditions.

A time lapse camera and light were mounted on the lander for the 2021 survey, to monitor the seabed and any depositional changes around the cable. Whilst the battery was drained after only 4 h, Fig. 5 illustrates that the images do provide some useful context. For the initial ebb to flood measured by the camera, no obvious scour was evident around the cable from the pictures taken. A small amount of sediment appeared on top of the cable after the initial settling of the lander on the bed, suggesting that there is flow separation occurring on the lee side of the cable with a flow speed of about 0.27 m s^{-1} (measured from AQD-1). The rippled sand bed visible in the background did not appear to move at all during the 4 h of footage taken, with a near bed flow speed up to 0.3 m s^{-1} ; this lack of sediment motion combined with the lack of any scour from the cable or lander feet suggests the sediments were largely immobile upon deployment in 2021.

3.1. Results: bed levels and cable burial

Depth-averaged mean velocities as measured by the upward facing Nortek Signature (Fig. 6a–b) are lower than the current speeds shown from the AWAC in Fig. 4c–d, due to the AWAC data being a near surface current speed rather than the depth-averaged. Peak depth-average mean current speeds in 2020 are around 0.6 m s^{-1} , and 0.5 m s^{-1} in 2021, and the phase lead of the velocity with respect to the water depth due to the standing tidal wave results in peak flows occurring during mid-flood and mid-ebb. The 2020 survey's two deployments can be seen either side of the gap in data around September 20th. For both deployments in 2020 the bed appears to rise by 0.2 m during the first two tides of each deployment (Fig. 6c). Gyroscope data from the instruments (Fig. 6e–f) suggests that the rear (ebb facing) side of the lander sank slightly during the first tide of both deployments in 2020. After one tide both deployments in 2020 show a stable pitch and roll. The change in lander angle is only enough (at most) to change the distance to the bed as measured by the ABS by 0.0024 m, indicating that the changes in bed elevation during this time are not due to the angle of the instruments changing. It is possible that if there is erosion around the legs of the lander this could be a source of sediment for deposition around the cable. The 2021 survey by comparison shows a gradual one-degree drift in pitch and roll during the survey. Although we cannot know for certain, it seems likely that the cable attached to the flood facing side of the lander actually prevented the lander from sinking at that end. The elevation of the cable (as measured by the ABS) during the deployments did not appear to change suggesting that the cable did not experience underscour and settlement. The change in pitch over time in 2021 has a similar trend to that of the bed level measured by the ABS, but a change in angle of 1° for a profile 1 m long would be nearly impossible to detect even with the ABS bin resolution of 0.5 cm. The simultaneous change in pitch and bed level is suggestive of the rear of the lander sinking slightly, which may be suspending some of the sediment which was measured in the surveys.

The higher resolution and more precise data of bed levels from of the ABS show that the bed reached the height of the cable during two ebb tides between September 21st and 22nd (Fig. 6c) – which was after the lander had stopped shifting. After these two tides, bed levels appear to stabilise at around 1 m away from the lander. The 2021 survey does not show a similar rapid response in bed level to the presence of the cable and instrument lander: with gradual deposition settling measurable during the deployment (Fig. 6d), up to 20 cm by the end of the survey.

Suspended sediment concentrations during the two deployments of

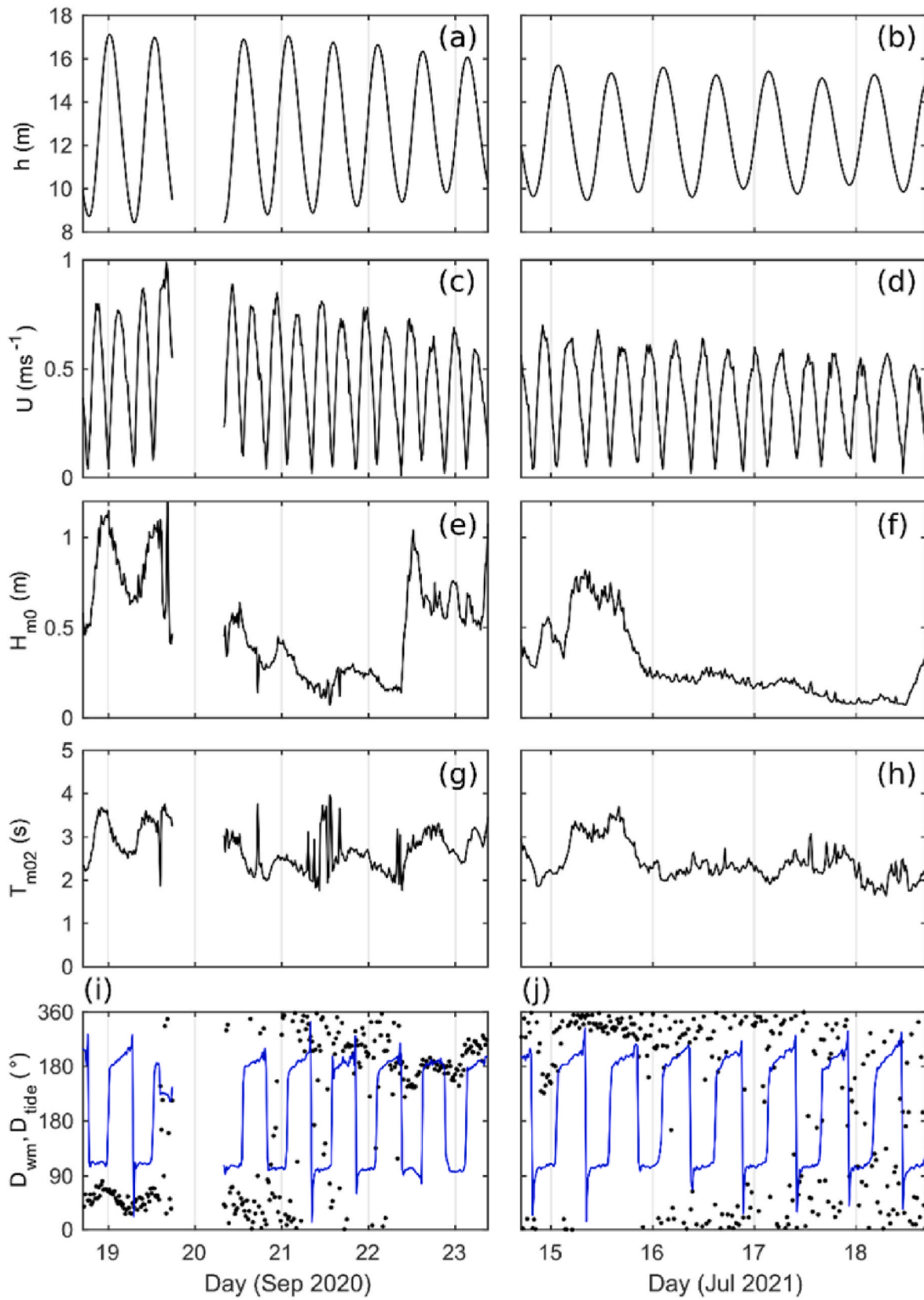


Fig. 4. Hydrodynamic forcing recorded by the AWAC during the field observations, September 2020 left panels, July 2021 right panels. (a, b) Water depth h ; (c, d) mean near-surface tidal current speed U ; (e, f) significant wave height H_{m0} ; (g, h) mean wave period T_{m02} ; and (i, j) mean wave direction D_{wm} (black dots) and tidal directions (blue line). All directions are from North.

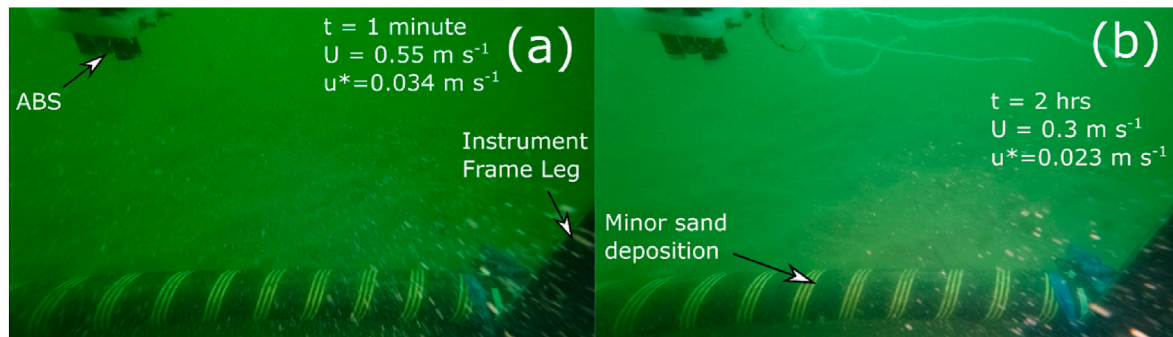


Fig. 5. Photographs from a lander-mounted time lapse camera, with lamp positioned to the right of the image, on July 14, 2021. (a) The first image of the lander on the seabed, the cable, part of the instrument lander leg, and the ABS can be seen. After 2 h (b) a small amount of sand can be seen resting on the cable, at this point no other deposition or scour is observed. A video of the photographs is provided in the supplementary material.

the 2020 survey exceed $\mathcal{O}(10^{-2}) \text{ kg m}^{-3}$ in the first two tides. This coincided with deposition of 0.2 m during both deployments indicating a consistent sequence of suspended sediment load and bed level change. The less energetic 2021 survey showed lower suspended sediment loads of $\mathcal{O}(10^{-3} - 10^{-4}) \text{ kg}^{-1} \text{ m}^{-3}$ (Fig. 6j), with little sediment suspended higher than 0.5 m above the seabed (Fig. 6h); conversely the 2020 survey showed clear flood and ebb suspensions in the entire ABS profile (Fig. 6g). The larger suspended sediment concentrations, and changes in the seabed at the start of the deployments suggests that these higher concentrations are more likely to be during a period of higher sediment mobility.

There is no obvious reason for the distinct difference in seabed response and sediment suspension between the 2020 and 2021 surveys. The seabed sediment particle size analyses did not identify any disparity between surveys which would account for a change in mobility of this magnitude. The position of the lander in the bedform field (Fig. 2) was on the lee side of a large bedform in 2021, and in a trough in 2020, therefore we would expect to see similar mobility affects from the known spatial variation of sediment mobility over marine dunes (Damveld et al., 2018). It is possible that the 2021 position is more sheltered to the flood tides, but this is not apparent in the mean velocity, nor near bed turbulence data measured from the lander. The most comparable tidal ranges between surveys are the largest tides in the 2021 survey and the end of the 2020 survey, and comparing these tides shows there was nearly an order of magnitude difference in suspended sediment loads for these similar tides. It is also notable that the distance to the bed first measured upon deployment, and the amount of movement of the lander were both greater in 2020 than 2021, suggesting the seabed was more cohesive and/or stronger in 2021, than 2020. This difference in overall mobility also appears to have affected how much and how quickly the self-burial processes occurred over the surveys. The next section investigates how burial of the cable itself by sediment accretion has affected the hydrodynamics over the cable which contribute to the self-burial.

3.2. Effects of cable burial on flow and turbulence

The presence of the lander and cable, moderated by the variation in bed level, should have impacted the form of the near bed turbulence and velocity profiles, with 2020 data less impacted than in 2021 due to greater burial of the cable in 2020. Fig. 7 assesses the shape of the mean velocity, turbulent kinetic energy profiles and suspended sediment concentrations over peak flood and ebb current speed of a tide for both lander deployments. Clear differences in the form of the mean velocity profiles for equivalent times during flood and ebb are evident (Fig. 7a and b). The flood conforms to the expected theoretical logarithmic form, whereas the ebb departs from this form becoming depth-invariant and even decreasing above $y = 0.6 \text{ m}$. For the 2021 comparison (Fig. 7b) with a greater cable exposure, the flow is faster above the cable, and

slower below the cable height. The TKE profiles (Fig. 7c and d) approximately follow the expected form during flood tides. During the ebbs the impact of the cable and lander higher in the water column are evident with high TKE values near and below the height of the cable between 0.8 and 1 m. For the more exposed cable 2021 data – near bed TKE is 50% higher compared to the mid profile.

Suspended sediment profiles in the 2020 survey demonstrate greater near bed suspension in the ebb tides compared to flood – in spite of the background suspended sediment concentration (indicated by SSC higher in the profile) being lower for ebb than flood. This indicates that the enhanced turbulence from the presence of the lander and cable is also enhancing suspended sediment concentrations. The 2021 survey, however, shows very little difference in profile shapes (Fig. 7b), and overall lower concentrations (Fig. 7f) – which are nearly equal in flood and ebb. TKE is similar or higher than the 2020 profiles indicating that the presence of the cable and lander is producing greater near bed turbulence in 2021 than 2020 (Fig. 7c–d), this enhanced (relative to flood tides) turbulence seems to have also increased the suspended sediment concentrations at the bed and near the cable, while concentration closer to the lander ($y = 0.4$) are equal in floods and ebbs (Fig. 7f).

It is clear that the two deployments show differing effects of the extra drag from the cable and instrument lander. The 2020 suspended sediment profiles are more greatly affected than 2021, yet the 2021 flow data are more obviously affected by the cable – likely due to the higher exposure of the cable above the seabed in the 2021 survey, whereas the 2020 survey showed evidence of cable burial due to sediment deposition (Fig. 8). This is further suggestive of a change in sediment mobility between surveys, and if so, suggests that overall bed sediment mobility affects cable burial processes more than the direct effects of turbulence generated by the cable itself.

3.3. Timing of burial and bed shear stress

The two Aquadopps on the lander arm (Fig. 3, AQD-1 and AQD-2) let us quantify the amount of shear coming directly from the cable and if the effects of cable burial modified it. Fig. 8a–b shows the estimate of the shear velocity (which drives sediment transport) derived from the TKE (equations (4) and (5)). The values for u^* from both Aquadopps during the flood tide are nearly identical whilst during ebbs u^* measured over the cable (AQD-2) is often (but not consistently) higher than that measured at the end of the lander arm (AQD-1). Ebb tides in the 2020 deployment in Fig. 8a and b shows higher TKE derived u^* from the Aquadopp over the cable in the first tides from all deployments by 20–30%, and 10–15% higher thereafter at peak ebb tide. In 2021, where there is less change in the bed elevation, there also is no obvious change in the flood/ebb asymmetry of peak u^* , further indicating that any morphological changes around the lander and cable were not altering the hydrodynamics much for this survey.

Normalising the shear velocity ($u^* = (\tau_b/\rho)^{0.5}$ with τ_b from Eq. (5))

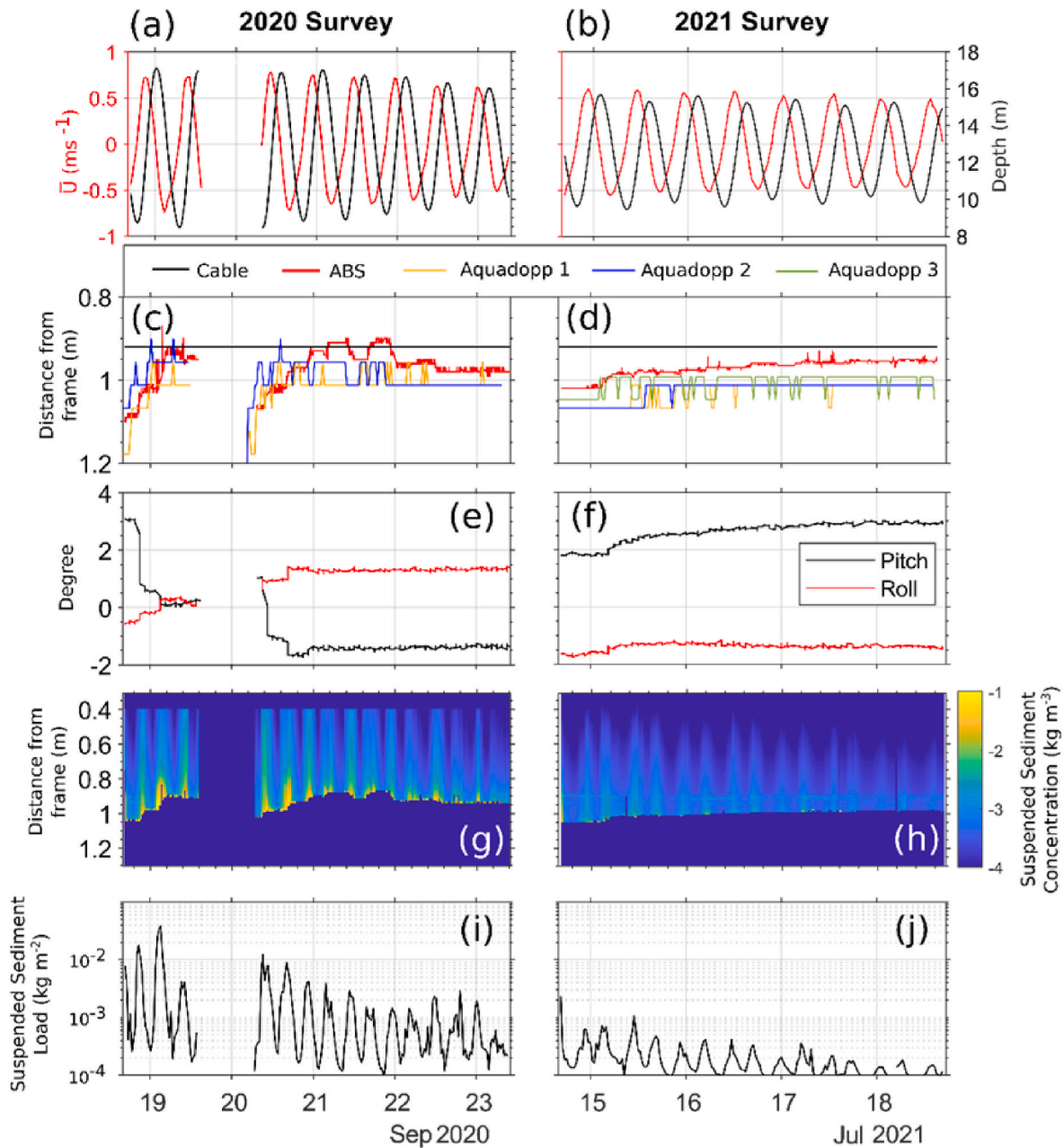


Fig. 6. (a & b) Burst average current speeds (red) and flow depths (black) from the upward facing Nortek Signature, with (c & d) downward facing acoustic instruments' measure of the bed level, relative to the top of the cable. (e & f) show the pitch and roll as measured by the upward facing signature (centrally positioned in the lander) from both deployments. (g & h) suspended sediment concentrations in log₁₀ colour scale, with suspended sediment loads (integrations of the profiles) shown in (i & j).

by the threshold of suspension in u^* form (from Eqs. (6)–(8)) shows that 84% of all measurements are above the threshold of suspension (Fig. 8c–d). As the diameter of the cable is known, the height of the seabed next to the cable, and the height of the cable itself above the seabed are measured by the ABS (within 10 cm of the cable), a direct measure of the embedment depth (E_c) can be produced. E_c is plotted in red on (Fig. 8c–d) and shows that much of the change in bed level is happening near peak bed shear stress of each tide. Fig. 8e–f quantifies the amount of deposition (or erosion) for each flood and ebb and demonstrates that aside from the first 1–2 tides of all deployments, if there is morphological change, flood tides erode whilst ebbs always deposit sediment. Such a process could either be movement of sediment from one side of the cable to the other over a tide, but as there are no

measurements of bed level of fine enough resolution (AQD-2 does have 1 beam on the ebb side of the cable), we cannot confirm or reject that hypothesis. The constant increase in burial in 2021 indicates that although transport was weak during these tides, some form of self-burial process was slowly occurring. In 2020 it is clear that there was a rapid deposition of sediment on either flood or ebb tide during the first two tides, followed by erosion of the sediment around the cable on floods and deposition on ebbs – indicating a rapid partial burial of the cable – followed by a volume of sand migrating to either side of the cable on each phase of the tide. The next section discusses these observations and places the results into a wider context of previous work about self-burial processes and cable scour.

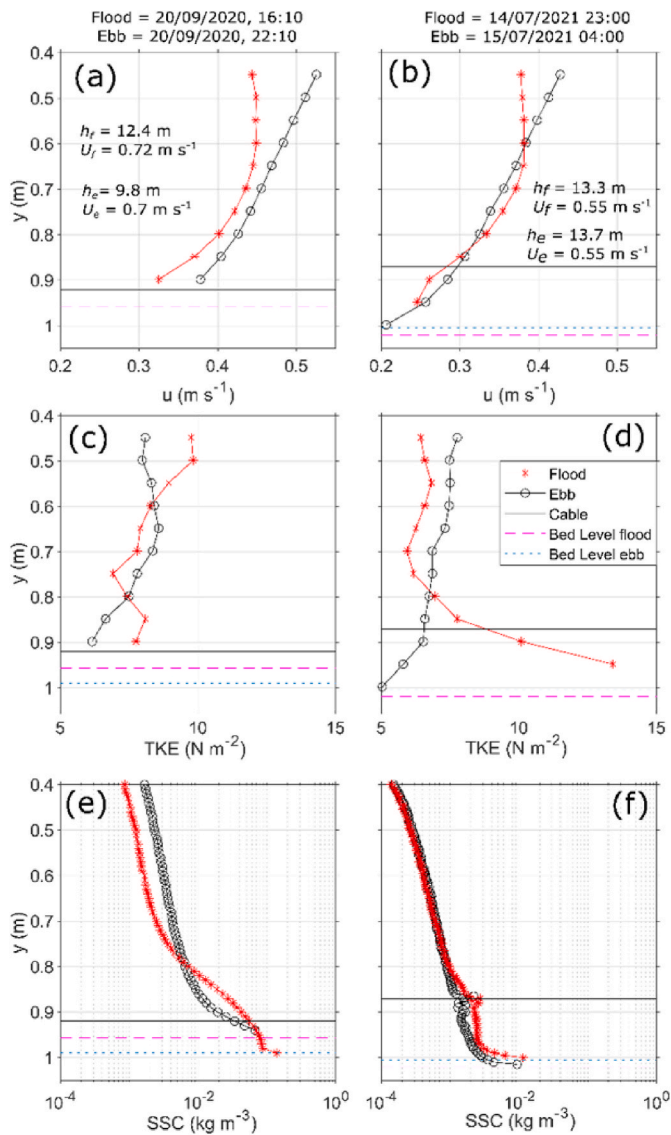


Fig. 7. Flood (black) and ebb (red) profiles of mean velocity (a, b), turbulent kinetic energy (c, d), and suspended sediment concentration (e, f), for the September 2020 (left) and July 2021 (right) deployments. Distances on the y axis are range from the Aquadopps 1 & 2 mounting elevation and indicate the top of the cable. The bed level changes between profiles in 2020 but is constant for the two profiles in the 2021 plots. Time the profiles were measured, and the depth averaged mean velocity from the upward facing Signature 1 000 are given as reference at the top of the figure.

4. Interpretation and discussion

Here we present the data from an offshore campaign where cable seabed interaction is monitored in real-time, quantifying mean flow, turbulence and suspended sediments. Whilst surveys of cables are commonplace, campaigns where laboratory style equipment and measurements are used to measure processes happening in high detail are rare, but provide insight into the interaction of cables and the seabed processes (Leckie et al., 2015, 2016, 2018), and biologically induced burial of pipelines (McLean et al., 2020, 2022), which produce new information and knowledge which can be used to improve cable and pipeline stability assessments. Whilst the spatial variability of seabed conditions is a key control on the potential for seabed mobilisation, and thus the burial process, the results we present here focus on the temporal variability in one location where the seabed is similar. Our study suggests that processes other than the typically used cable diameter,

embedment depth and mean flow, control the burial process. In the section below we discussed these processes, and how they are enough to modify the rate and intensity of cable burial.

4.1. Scour vs deposition

For a deployment under relatively fast currents and a mobile sand bed, it was largely expected at the start of the surveys that scour would occur beneath the cable. Yet the observations during this study all indicate that no scour occurred, and that instead burial processes dominated. To confirm the observations of no scour under the central portion of the cable, the breakthrough for tunnel scour in granular sediment was evaluated using the formula fitted to laboratory experiments by Sumer and Fredsøe (2002). Values for the reference velocity at the top of the cable were taken from the ADCP bin closest to the cable from AQD-2 (as is required by the model), the results are shown in Fig. 9a.

Plotting U_{ref}^2 also demonstrates a large difference in velocity above the cable between deployments (Fig. 9b & c), with the 2021 survey U_{ref}^2 about half that of the 2020 data, despite the neap tides in 2020 (when transport did occur) and spring tides in 2021 (with little observed transport) having similar tidal ranges. This difference in near bed flow speed between deployments could be due to greater sheltering from the flood tides due to the position of the 2021 lander on a lee slope of a larger bedform compared to the more exposed position in 2020 (cf. Fig. 2e). Whilst the frame itself may have been in a more sheltered location in 2021, the greater exposure of the cable to the flow due to lower embedment depths did produce higher TKE around the cable than in 2020 (Fig. 7c–d), suggesting that the effects of the cable on the near bed flow are still important even though U_{ref}^2 (and therefore risk of scour) was lower in 2021.

4.2. Seabed mobility

One of the surprising findings from the surveys was the differing responsiveness of the bed and the suspended sediment concentrations. To investigate this further, the suspended sediment loads (C) from each survey are plotted against u^* estimated (Fig. 10) from the AQD-1 using the TKE method (Soulsby and Dyer, 1981). The empirical threshold of motion (in u^*) of the sediments is 0.0134 m s^{-1} and is used to normalise the x axis. Whilst there is nearly an order of magnitude scatter in C per value of u^*/u_{sus}^* , there is a clear separation in the distribution of C between each year's data (Fig. 10a). To illustrate how different the seabed mobility was between surveys, three different values for u_{sus}^* across a broad range {0.01 0.02 0.04} were applied to the 2021 data (Fig. 9b). These thresholds of motion correspond to the grain sizes {45 400 1250} μm . An adjusted u_{sus}^* of 0.02 collapses the 2021 data onto the 2020 data and is equivalent to a sand grain diameter of 400 μm , 1.63x larger than the D_{50} from both year's grab samples, but clearly not representative of the seabed sediments which were measured from the PSD of the grab sample.

With a direct estimate of the bed shear stress from near bed turbulence data applied and variation in grain size distribution minimal, we see very few reasons why there would be such a difference in seabed mobility, so in the following section we suggest several hypotheses which may explain the large difference in seabed mobility. A bimodal sediment mixture can alter the threshold of motion by the magnitude observed through the hiding-exposure effect (McCarron et al., 2019). The grab sample sediment sizes $\geq 900 \mu\text{m}$ made up $< 0.1\%$ of the grain size distributions and are therefore too few to affect the mobility of the sediment via this process, and these distributions are reasonably similar between both years' grab samples. So, whilst this process does occur in the region, our data do not support it as a major factor at the survey site. Adding in a small amount of coarser sediment into the grain size

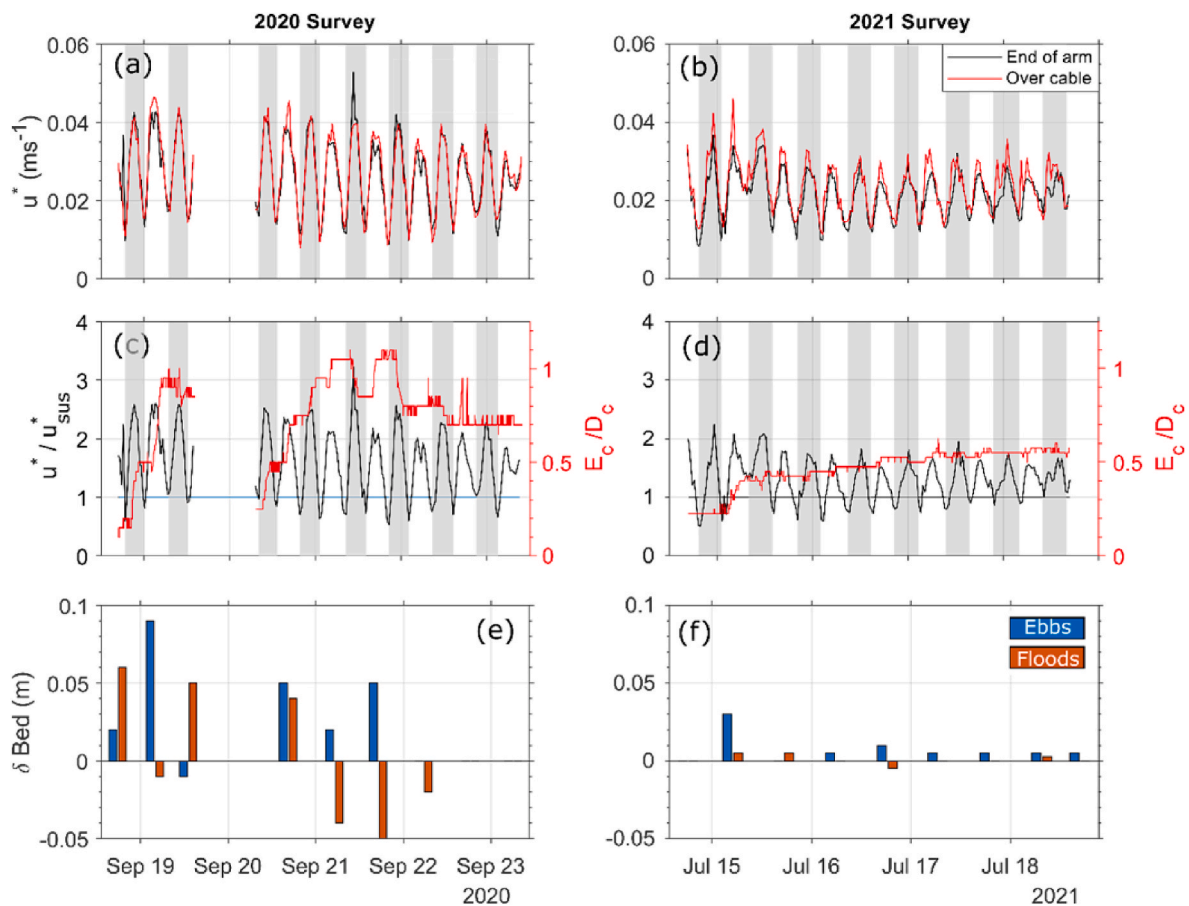


Fig. 8. (a,b) u^* derived from the TKE method of estimating bed shear stress for both Aquadopps. Estimates from over the cable (AQD-2) are often higher in ebbs compared to the instrument at the end of the frames arm (AQD-1). Shaded areas indicate flood tides. (c&d), bed levels plotted with u^* from the over the cable Aquadopp scaled by the initiation of suspension for the bed sediments, (e&f) change in the embedment of the cable over individual flood and ebb tides, positive values indicate deposition, negative is erosion.

distribution (whilst keeping it unimodal) has demonstrated a change to mobility in laboratory experiments (MacKenzie and Eaton, 2017). Such fine scale variability is not impossible in the environment we survey, but an introduction of new coarser sediment into the system seems unlikely given the location of the site and the grab samples obtained. The “armouring” process hypothesised by (MacKenzie and Eaton, 2017), is a possible candidate as an explanation for our results but little work has been conducted on the armouring of sand only sediments. Near bed sorting processes like this, and the variability in seabed mobility they produce, is often considered a form of “natural variability” in seabed sediment dynamics as it is often too difficult to measure. In fluvial environments, particularly coarse-grained rivers (Dietrich et al., 1989; Vericat et al., 2006), more work has been concluded on this topic due to the ease of measuring the active layer of sediment transport (Hassan et al., 2020; Pähntz et al., 2020), whilst subtidal work has often focused on broader changes of mobility due to fines (Amos et al., 1997; Thompson et al., 2011). We suggest that changes in the mobility of unimodal sands could be detectable in long term (>1 month) long field surveys of seabed mobility where a drift in the relationship between bed shear stress and suspended sediment concentrations would occur over these timescales due to near bed sorting processes modifying the top layer of sediment.

Lastly, one other cause which can alter sediment mobility, which was not measure in these surveys, is the presence of extracellular polymeric substance (EPS) producing organisms. Recent work has illustrated that EPS can influence sediment mobility by an order of magnitude either from the EPS itself (Chen et al., 2017a), or from the fines that EPS introduce into the bed (Chen et al., 2017b; Hope et al., 2020). It is

notable that the camera pictures on the 2021 frame (Fig. 5) showed green seawater which should indicate the presence of plentiful marine microorganisms. Seafloor measurements of EPS are rare, with most measurements in intertidal and riverine environments where access is much easier (e.g., Chen et al., 2017a,b; Hope et al., 2020; Paterson, 1989; Underwood and Paterson, 1993). Furthermore, recent intertidal surveys have shown that even small (1–2% by mass) quantities of mud and/or clay can alter bed mobility by 2–3x (Hope et al., 2020; Lichtman et al., 2018), so a similar scale of the changes in mobility found in the current study. Further work is needed to confidently state if EPS, mud and clay content are components of the sea floor system which are moderating the in-seabed mobility seen in the present study. From our own samples, sediment sizes <63 μm made up < 1% of the grab sample (by mass) but as the sampling strategy was designed for sand and coarser sizes, clay, mud and silt could have been lost in the process. Visual surveys of sub-tidal dune beds have also shown high spatial variability in grain size, mud and possible biological effects on the seabed (Damveld et al., 2018). It seems plausible that our grab samples could have missed, by chance, this small-scale variability. As such we encourage a spatial visual and grab sample survey to be sure of ground conditions upon deployment, when subtidal bedforms are present.

4.3. Turbulence modification and self-burial

The present surveys allow us to directly investigate the amplification of shear using AQD-2 directly above the cable and compare it to the ambient shear stress recorded by AQD-1. Fig. 11 shows the ratio of the peak tidal (for floods and ebbs) shear velocity from these two

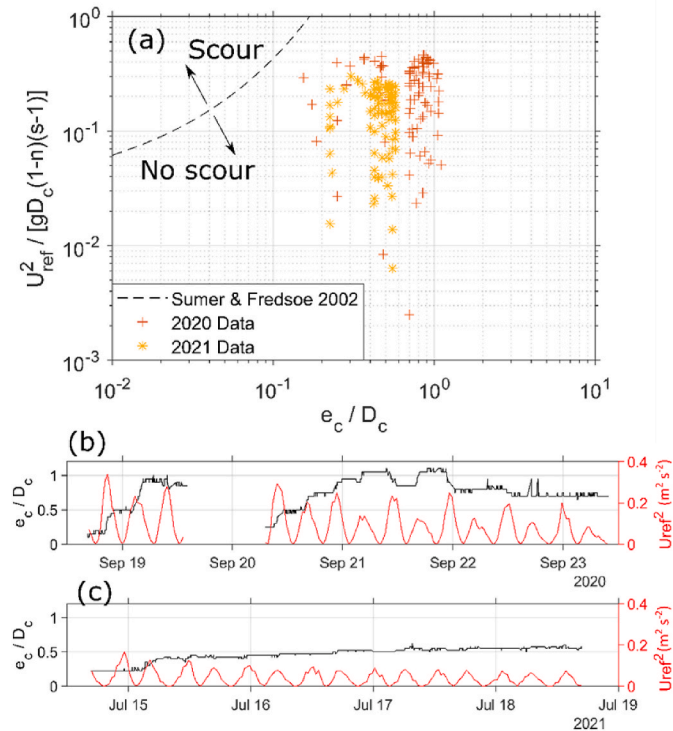


Fig. 9. (a) Dashed line is the onset of scour under a rigid cable on the seabed (Equation (1); Sumer and Fredsøe, 2002) and the values measured in this study. (b) and (c) show the values in (a) plotted with time for the 2020 and 2021 deployments respectively.

Aquadopps, plotted with the embedment ratio. Here we see that in the 2020 survey, as the embedment ratio increased to well over 50%, the ratio of peak shear stresses reduces and even becomes <1, indicating that at higher embedment (near unity) the turbulence near the cable is actually lower than in the free stream. The 2021 survey is more inconclusive, embedment reaches >50%, but the ratio of peak stresses is not clearly altered in response – turbulence near the cable clearly remains

amplified during both floods and ebbs. This comparison suggests embedment depths much greater than 50% are needed to noticeably reduce turbulence over a cable in this kind of environment.

Previous research has found that for embedment depths of 50% or greater, the reverse flow in the lee wake (Fig. 1) moved sediment towards a pipeline (Chiew, 1990). From our surveys, this kind of self-reinforcing process appears to occur for all conditions regardless of the embedment depth – notably in 2021 where gradual deposition around the cable was observed with a starting embedment depth of 20%. So, we suggest that under the conditions observed during our surveys, cables Zhao et al. (2015) showed a net influx of sediment in the volume around a pipeline was a large contributing factor to sedimentation, and the beginning of the 2020 survey seems to support this concept on a real in-field example, with suspended sediment loads up to 0.04 kg m^{-3} , and as concentration dropped during the survey flood tides started to erode rather than deposition sediment.

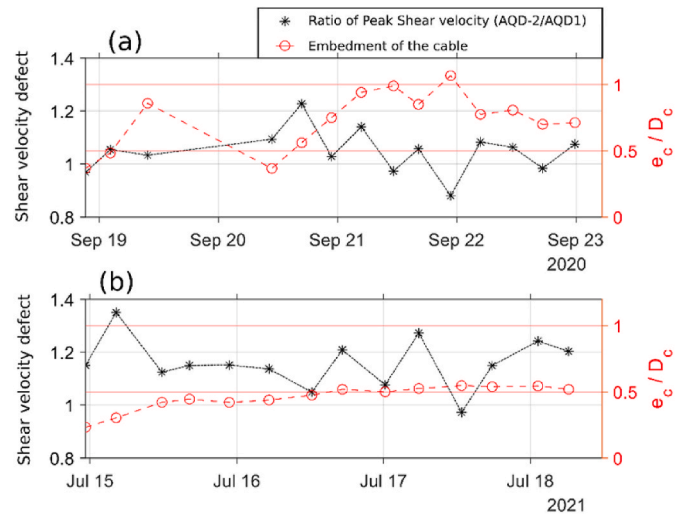


Fig. 11. the ratio of peak shear velocity (AQDP-2 over cable/AQDP-1 end of arm) per flood and ebb, with the embedment of the cable shown on the right axis, for 2020 (a) and 2021 (b) surveys. Values on the left y axis >1 show higher u^* occurred during ebb tides.

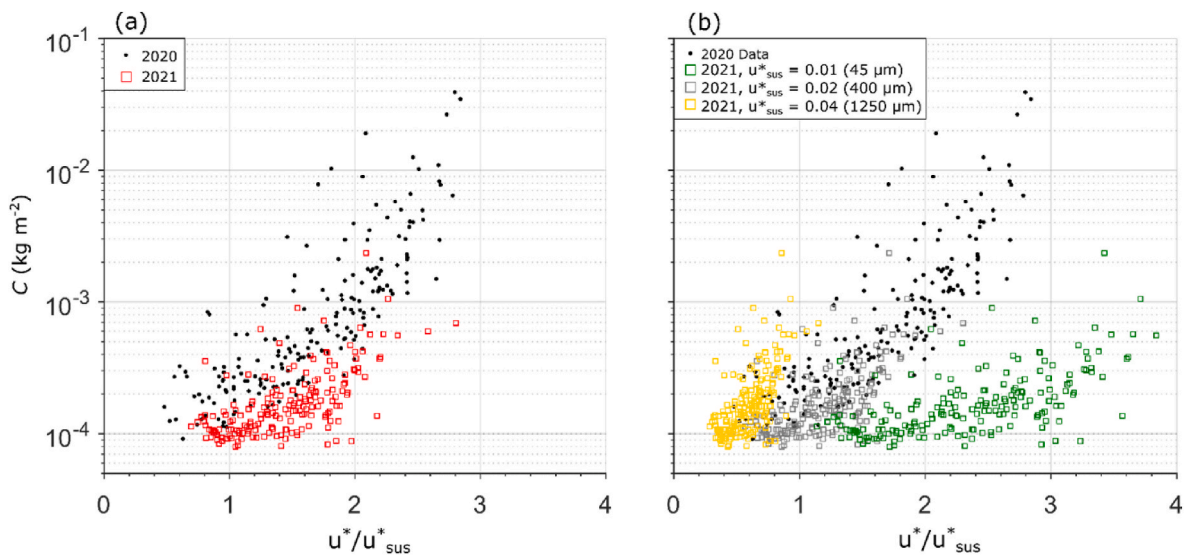


Fig. 10. (a) Scatter plot of burst average suspended sediment load (C , kg m^{-2}) versus the normalised shear velocity for each burst, with a value of 0.0134 m s^{-1} for u_{SUS}^* estimated from eqs. (6) and (7). Panel (b) shows the same C , but as a sensitivity check for the 2021 data three different values for u_{SUS}^* (equivalent grain size at 10°C are given in parenthesis) were used to normalise u^* .

Our repeated multibeam surveys in 2021 showed no measurable sediment build up around the lander and sediment suspension, even with the enhanced turbulence produced by the cable. The results in Fig. 11 confirm that for embedment by sediment build-up of up to around 50% the local shear velocity is enhanced by 15–20%, and with the streamlining effect of 75–100% embedment value of local shear stress is about the same as the ambient. It appears that for the 2021 conditions at the site, an increase in peak shear stress at the cable location of nearly 40% above ambient level was insufficient to mobilise much sediment, even though nearly all the measurements were above the threshold of motion and suspension as calculated from standard equations (Eqs. (4)–(6)). This combination of factors strongly suggests that an unmeasured differential seabed mobility between 2020 and 2021 was affecting the relationship between bed shear stress and suspended sediment concentration, and subsequently the process of cable burial, and that future work is required to fully understand what controls mobility – even when the sediments are uniform and well sorted, with <1% fines or coarse fractions.

5. Conclusions

Field surveys conducted in a region of existing and expanding offshore renewable energy infrastructure quantified the mean flow, turbulence, sediment suspension and bed levels around a section of typical subsea electricity cable. The survey results found that the initial embedment depth of the cable and the flow conditions above the cable upon deployment were good indications of the trajectory of the bed response. The bedform field at the site indicated that there was sediment mobility and hence at the start of all deployments as the cable was placed in contact with the bed scour under the cable did not occur, and self-burial processes through sedimentation existed through the surveys. Subsequent surveys in 2021 indicated a self-burial process still occurred with little sediment in suspension and despite enhanced turbulence originating from the cable.

Despite the location of both deployments being similar, there was a large difference in the seabed response and the suspended sediment concentrations between the two surveys, and there is no clear answer to why. It is suggested that the larger tides and typical wave conditions at the start of the 2020 survey produced a more mobile seabed compared to the calmer (but not atypical) conditions during which the 2021 survey occurred. Paradoxically, the 2021 survey's lack of sediment suspension and seabed elevation changes lead to a more exposed cable and an enhancement of 30–40% more turbulence produced by the cable compared to ambient flow. However, this enhanced turbulence did not seem to affect sediment suspension or cable burial, despite peak bed shear stresses being twice the initiation of motion or suspension for the sediments. In the more mobile 2020 surveys, cable burial reduced the excess turbulence produced by the cable to an immeasurable difference to the ambient condition as embedment depth tended to unity. Once this state was reached the seabed around the cable varied on each phase of the tide. For all surveys, deposition occurred around the cable – but at very different rates dependent on forcing and local bed conditions. The turbulence induced from the cable itself appeared to lead to locally increased sedimentation around the cable.

Author credit statement

Christopher A. Unsworth: Experiments, Data analysis and writing Review and editing, All authors discussed the results and contributed to the final manuscript. Martin J. Austin: Conceptualization and research plan, Experiments, Data analysis and writing Review and editing, All authors discussed the results and contributed to the final manuscript. Katrien J.J. Van Landeghem: Conceptualization and research plan, Experiments, Data analysis and writing Review and editing, All authors discussed the results and contributed to the final manuscript. Amelia J. Couldrey: Conceptualization and research plan, Data analysis and

writing Review and editing, All authors discussed the results and contributed to the final manuscript. Richard J.S. Whitehouse: Conceptualization and research plan, Data analysis and writing Review and editing, All authors discussed the results and contributed to the final manuscript. Ben Lincoln: Conceptualization and research plan, All authors discussed the results and contributed to the final manuscript. Siobhan Doole: Conceptualization and research plan, All authors discussed the results and contributed to the final manuscript. Peter Worrall: Conceptualization and research plan, All authors discussed the results and contributed to the final manuscript.

Declaration of competing interest

The authors declare that they have no known competing financial interests or personal relationships that could have appeared to influence the work reported in this paper.

Data availability

Data will be made available on request.

Acknowledgements

This work was funded by the ESPRC Supergen ORE Flexible Fund grant FF 2020-1095 and the ECOWind-ACCELERATE project (NE/X008886/1) Project. Additional support was provided by the Smart Efficient Energy Centre (SEEC) funded by the Welsh European Funding Office (WEFO) as part of the European Regional Development Fund (ERDF). AJC and RJSW also acknowledge provision of matching funds from the HR Wallingford strategic Scour Research Programme. The team thanks Ben Powell, Aled Owen, and the crew of the RV Prince Madog for facilitating this fieldwork under difficult working conditions due to COVID-19 restrictions.

Appendix A. Supplementary data

Supplementary data to this article can be found online at <https://doi.org/10.1016/j.coastaleng.2023.104309>.

References

- Amos, C.L., Feeney, T., Sutherland, T.F., Luternauer, J.L., 1997. The stability of fine-grained sediments from the Fraser river delta. *Estuar. Coast Shelf Sci.* 45.
- Ardelean, M., Minnebo, P., 2023. The suitability of seas and shores for building submarine power interconnections. *Renewable and Sustainable Energy Reviews* 176. <https://doi.org/10.1016/j.rser.2023.113210>.
- Bennett, S.J., Best, J.L., 1995. Mean flow and turbulence structure over fixed, two-dimensional dunes: implications for sediment transport and bedform stability. *Sedimentology* 42, 491–513.
- Biron, P.M., Robson, C., Lapointe, M.F., Gaskin, S.J., 2004. Comparing different methods of bed shear stress estimates in simple and complex flow fields. *Earth Surf. Process. Landforms* 29 (11), 1403–1415. <https://doi.org/10.1002/esp.1111>.
- Chen, X.D., Zhang, C.K., Paterson, D.M., Thompson, C.E.L., Townend, I.H., Gong, Z., Zhou, Z., Feng, Q., 2017a. Hindered erosion: the biological mediation of noncohesive sediment behaviour. *Water Resour. Res.* 53 (6), 4787–4801. <https://doi.org/10.1002/2016WR020105>.
- Chen, X.D., Zhang, C.K., Zhou, Z., Gong, Z., Zhou, J.J., Tao, J.F., Paterson, D.M., Feng, Q., 2017b. Stabilizing effects of bacterial biofilms: EPS penetration and redistribution of bed stability down the sediment profile. *J. Geophys. Res.: Biogeosciences* 122 (12), 3113–3125. <https://doi.org/10.1002/2017JG004050>.
- Chiew, B.Y., 1990. Mechanics of local scour around submarine pipelines. *J. Hydraul. Eng.* 4 (515), 515–529. [https://doi.org/10.1061/\(ASCE\)0733-429\(1990\)116](https://doi.org/10.1061/(ASCE)0733-429(1990)116).
- Clare, M.A., Yeo, I.A., Bricheno, L., Aksenov, Y., Brown, J., Haigh, I.D., Wahl, T., Hunt, J., Sams, C., Chaytor, J., Bett, B.J., Carter, L., 2023. Climate change hotspots and implications for the global subsea telecommunications network. In: *Earth-Science Reviews*, 237. <https://doi.org/10.1016/j.earscirev.2022.104296>.
- Couldrey, A.J., Benson, T., Knaapen, M.A.F., Marten, K.V., Whitehouse, R.J.S., 2020. Morphological evolution of a barchan dune migrating past an offshore wind farm foundation. *Earth Surf. Process. Landforms* 45 (12), 2884–2896. <https://doi.org/10.1002/esp.4937>.
- Damgaard, M., Andersen, L.v., Ibsen, L.B., 2015. Dynamic response sensitivity of an offshore wind turbine for varying subsoil conditions. *Ocean. Eng.* 101, 227–234. <https://doi.org/10.1016/j.oceaneng.2015.04.039>.

- Damveld, J.H., van der Reijden, K.J., Cheng, C., Koop, L., Haakma, L.R., Walsh, C.A.J., et al., 2018. Video transects reveal that tidal sand waves affect the spatial distribution of benthic organisms and sand ripples. *Geophys. Res. Lett.* 45 (21), 837–846. <https://doi.org/10.1029/2018GL079858>.
- Dey, S., Paul, P., Padhi, E., 2020. Conditional spatially averaged turbulence and dispersion characteristics in flow over two-dimensional dunes. *Phys. Fluids* 32 (6). <https://doi.org/10.1063/5.0008380>.
- Dietrich, W.E., Kirchner, J.W., Ikeda, H., Iseya, F., 1989. Sediment supply and the development of the coarse surface layer in gravel-bedded rivers. *Nature* 340 (6230), 215–217. <https://doi.org/10.1038/340215a0>.
- Dyer, K.R., 1986. *Coastal and Estuarine Sediment Dynamics*. John Wiley & Sons, Chichester, U. K.
- El Mountassir, O., Strang-Moran, C., 2018. *Offshore Wind Subsea Power Cables. Installation, Operation and Market Trends*. University of Hull.
- Guerra, M., Thomson, J., 2017. Turbulence measurements from five-beam acoustic Doppler current profilers. *J. Atmos. Ocean. Technol.* 34 (6), 1267–1284. <https://doi.org/10.1175/JTECH-D-16-0148.1>.
- Hassan, M.A., Saletti, M., Johnson, J.P.L., Ferrer-Boix, C., Venditti, J.G., Church, M., 2020. Experimental insights into the threshold of motion in alluvial channels: sediment supply and streambed state. *J. Geophys. Res.: Earth Surf.* 125 (12) <https://doi.org/10.1029/2020JF005736>.
- Herbert, C.M., Alexander, J., Martínez de Álvaro, M.J., 2015. Back-flow ripples in troughs downstream of unit bars: formation, preservation and value for interpreting flow conditions. *Sedimentology* 62 (7), 1814–1836. <https://doi.org/10.1111/sed.12203>.
- Hope, J.A., Malarkey, J., Baas, J.H., Peakall, J., Parsons, D.R., Manning, A.J., Bass, S.J., Lichtman, I.D., Thorne, P.D., Ye, L., Paterson, D.M., 2020. Interactions between sediment microbial ecology and physical dynamics drive heterogeneity in contextually similar depositional systems. *Limnol. Oceanogr.* 1–17. <https://doi.org/10.1002/lno.11461>.
- Kim, S.-C., Friedrichs, C.T., Maa, J.P.-Y., Wright, L.D., 2000. Estimating bottom stress in tidal boundary layer from acoustic Doppler velocimeter data. *J. Hydraul. Eng.* 126 (6), 399–406. [https://doi.org/10.1061/\(asce\)0733-9429\(2000\)126:6\(399\)](https://doi.org/10.1061/(asce)0733-9429(2000)126:6(399)).
- Leckie, S.H.F., Draper, S., White, D.J., Cheng, L., Fogliani, A., 2015. Lifelong embedment and spanning of a pipeline on a mobile seabed. *Coast Eng.* 95, 130–146. <https://doi.org/10.1016/j.coastaleng.2014.10.003>.
- Leckie, S.H.F., Mohr, H., Draper, S., McLean, D.L., White, D.J., Cheng, L., 2016. Sedimentation-induced burial of subsea pipelines: observations from field data and laboratory experiments. *Coast Eng.* 114, 137–158. <https://doi.org/10.1016/j.coastaleng.2016.04.017>.
- Leckie, S.H.F., Draper, S., White, D.J., Cheng, L., Griffiths, T., Fogliani, A., 2018. Observed changes to the stability of a subsea pipeline caused by seabed mobility. *Ocean Eng.* 169 (January), 159–176. <https://doi.org/10.1016/j.oceaneng.2018.07.059>.
- Lefebvre, A., Herrling, G., Becker, M., Zorndt, A., Krämer, K., Winter, C., 2022. Morphology of estuarine bedforms, wester estuary, Germany. *Earth Surf. Process. Landforms* 47 (1), 242–256. <https://doi.org/10.1002/esp.5243>.
- Lichtman, I.D., Baas, J.H., Amoudry, L.O., Thorne, P.D., Malarkey, J., Hope, J.A., Peakall, J., Paterson, D.M., Bass, S.J., Cooke, R.D., Manning, A.J., Davies, A.G., Parsons, D.R., Ye, L., 2018. Bedform migration in a mixed sand and cohesive clay intertidal environment and implications for bed material transport predictions. *Geomorphology* 315, 17–32. <https://doi.org/10.1016/j.geomorph.2018.04.016>.
- MacKenzie, L.G., Eaton, B.C., 2017. Large grains matter: contrasting bed stability and morphodynamics during two nearly identical experiments. *Earth Surf. Process. Landforms* 42 (8), 1287–1295. <https://doi.org/10.1002/esp.4122>.
- Mayall, R.O., McAdam, R.A., Whitehouse, R.J.S., Burd, H.J., Byrne, B.W., Heald, S.G., et al., 2020. Flume tank testing of offshore wind turbine dynamics with foundation scour and scour protection. *J. Waterw. Port. Coast. Ocean Eng.* 146 (5), 1–17. [https://doi.org/10.1061/\(asce\)jww.1943-5460.0000587](https://doi.org/10.1061/(asce)jww.1943-5460.0000587).
- McCarron, C.J., van Landeghem, K.J.J., Baas, J.H., Amoudry, L.O., Malarkey, J., 2019. The hiding-exposure effect revisited: a method to calculate the mobility of bimodal sediment mixtures. *Mar. Geol.* 410 (November 2018), 22–31. <https://doi.org/10.1016/j.margeo.2018.12.001>.
- McLean, S.R., Wolfe, S.R., Nelson, J.M., 1999. Spatially averaged flow over a wavy boundary revisited. *J. Geophys. Res.: Oceans* 104 (C7), 15743–15753. <https://doi.org/10.1029/1999jc900116>.
- McLean, D.L., Vaughan, B.I., Malseed, B.E., Taylor, M.D., 2020. Fish-habitat associations on a subsea pipeline within an Australian Marine Park. *Mar. Environ. Res.* 153 (October 2019), 104813 <https://doi.org/10.1016/j.marenvres.2019.104813>.
- McLean, D., Speed, C.W., Birt, M.J., Colquhoun, J., Case, M., Stowar, M., Bond, T., Ierodiakonou, D., Whitmarsh, S.K., Taylor, M.D., Wines, S., Booth, D.J., Fowler, A. M., Vaughan, B.I., 2022. Habitat value of subsea wells and pipelines for fishery target species in Australia. *Front. Mar. Sci.* 9 (August), 1–23. <https://doi.org/10.3389/fmars.2022.960496>.
- Mohr, H., Draper, S., Cheng, L., White, D.J., 2016. Predicting the rate of scour beneath subsea pipelines in marine sediments under steady flow conditions. *Coast Eng.* 110, 111–126.
- Nowell, A., Church, M.A., 1979. Turbulent flow in a depth-limited boundary layer. *Journal of Geophysical Research-Oceans* 84 (C8), 4816–4824.
- Pächt, T., Clark, A.H., Valyrakis, M., Durán, O., 2020. The Physics of Sediment Transport Initiation, Cessation, and Entrainment across Aeolian and Fluvial Environments. *Reviews of Geophysics*. Blackwell Publishing Ltd. <https://doi.org/10.1029/2019RG000679>.
- Paterson, D., 1989. Short-term in the erodibility of intertidal cohesive sediments related to the migratory behavior of epipelagic diatoms. *Limnol. Oceanogr.* 34 (1), 223–234. <https://doi.org/10.2307/2837074>.
- Pope, N.D., Widdows, J., Brinsley, M.D., 2006. Estimation of bed shear stress using the turbulent kinetic energy approach—a comparison of annular flume and field data. *Continental Shelf Res.* 26 (8), 959–970. <https://doi.org/10.1016/j.csr.2006.02.010>.
- Rippeth, T.P., Williams, E., Simpson, J.H., 2002. Reynolds stress and turbulent energy production in a tidal channel. *J. Phys. Oceanogr.* 32 (4), 1242–1251. [https://doi.org/10.1175/1520-0485\(2002\)032<1242:RSATEP>2.0.CO;2](https://doi.org/10.1175/1520-0485(2002)032<1242:RSATEP>2.0.CO;2).
- Soulsby, R., 1997. *Dynamics of Marine Sands*. Thomas Telford Publications, London, UK.
- Soulsby, R.L., Dyer, K.R., 1981. The form of the near-bed velocity profile in a tidally accelerating flow. *J. Geophys. Res.* 86 (C9), 8067. <https://doi.org/10.1029/JC086iC09p08067>.
- Sumer, B.M., Fredsøe, J., 2001. Scour around pile in combined waves and current. *J. Hydraul. Eng.* 127 (5), 403–411.
- Sumer, M., Fredsøe, J., 2002. *The Mechanics of Scour in the Marine Environment*, vol. 17. World Scientific.
- Sumer, B.M., Kirca, V.S.O., 2022. Scour and liquefaction issues for anchors and other subsea structures in floating offshore wind farms: a review. *Water Sci. Eng.* 15 (1), 3–14. <https://doi.org/10.1016/j.wse.2021.11.002>.
- Sumer, B.M., Truelsen, C., Sichmann, T., Fredsøe, J., 2001a. Onset of scour below pipelines and self-burial. *Coast Eng.* 42.
- Sumer, B.M., Whitehouse, R.J.S., Tørum, A., 2001b. Scour around coastal structures: a summary of recent research. *Coast Eng.* 44 (2), 153–190. [https://doi.org/10.1016/S0378-3839\(01\)00024-2](https://doi.org/10.1016/S0378-3839(01)00024-2).
- Thompson, C.E.L., Couceiro, F., Fones, G.R., Hellsby, R., Amos, C.L., Black, K., et al., 2011. In situ flume measurements of resuspension in the North Sea. *Estuar. Coast Shelf Sci.* 94 (1), 77–88. <https://doi.org/10.1016/j.ejss.2011.05.026>.
- Thorne, P.D., Hanes, D.M., (2002). A review of acoustic measurement of small-scale sediment processes, *Continental Shelf Research*, (22), 4,603–632.
- Thorne, P.D., Meral, R., 2008. Formulations for the scattering properties of suspended sandy sediments for use in the application of acoustics to sediment transport processes. *Continental Shelf Res.* 28 (2), 309–317. <https://doi.org/10.1016/j.csr.2007.08.002>.
- Underwood, G.J.C., Paterson, D.M., 1993. Seasonal changes in diatom biomass, sediment stability and biogenic stabilization in the Severn Estuary. *J. Mar. Biol. Assoc. U. K.* 73 (4), 871–887. <https://doi.org/10.1017/S0025315400034780>.
- Unsworth, C.A., Parsons, D.R., Hardy, R.J., Reesink, A.J.H., Best, J.L., Ashworth, P.J., Keevil, G.M., 2018. The impact of nonequilibrium flow on the structure of turbulence over river dunes. *Water Resour. Res.* 54 (9), 6566–6584. <https://doi.org/10.1029/2017WR021377>.
- van Rijn, L., 1993. *Principles of Sediment Transport in Rivers, Estuaries and Coastal Seas*. Aqua Publications.
- Vericat, D., Batalla, R.J., Garcia, C., 2006. Breakup and reestablishment of the armour layer in a large gravel-bed river below dams: the lower Ebro. *Geomorphology* 76 (1–2), 122–136. <https://doi.org/10.1016/j.geomorph.2005.10.005>.
- Whitehouse, R.J.S., Draper, S., 2020. Sediment transport and scour in the ocean environment – knowledge and future directions. In: Westgate, Zack (Ed.), *Proceedings of the 4th International Symposium on Frontiers in Offshore Geotechnics*, ISFOG. Deep Foundations Institute, pp. 178–205.
- Williams, J.J., Rose, C.P., Thorne, P.D., O'Connor, B.A., Humphrey, J.D., Hardcastle, P. J., et al., 1999. Field observations and predictions of bed shear stresses and vertical suspended sediment concentration profiles in wave-current conditions. *Continental Shelf Res.* 19 (4), 507–536. [https://doi.org/10.1016/S0278-4343\(98\)00098-3](https://doi.org/10.1016/S0278-4343(98)00098-3).
- Zhang, J., Chen, Y., Jia, F., Zhou, Y., Li, H., Li, C., Huang, X., Guo, Q., 2021. Damage analysis of suspended submarine cable under current force based on finite element simulation. In: *ICSDM 2021 - 2nd International Conference on Sensing, Measurement and Data Analytics in the Era of Artificial Intelligence*. Institute of Electrical and Electronics Engineers Inc. <https://doi.org/10.1109/ICSDM53520.2021.9670552>.
- Zhao, F., Griffiths, T., Shen, W., Draper, S., An, H., Leggoe, J., Carneiro, D., 2015. Sediment attractors: seabed shear stress shadows around subsea pipelines cause net sediment accretion. In: *Proceedings of the ASME 2015 34th International Conference on Ocean, Offshore and Arctic Engineering*. St John's, Newfoundland, p. 13.